Climate Dynamics (1997) 13: 547–560

Climate Dynamics
© Springer-Verlag 1997

On aspects of the concept of radiative forcing

P. M. de F. Forster, R. S. Freckleton, K. P. Shine

Department of Meteorology, Reading University, Whiteknights, PO Box 239, Reading, RG6 6BB, UK

Received: 25 October 1996/Accepted: 14 April 1997

Abstract. The concept of radiative forcing has been extensively used as an indicator of the potential importance of climate change mechanisms. It allows a first order estimate of the global-mean surface temperature change; and it is possible to compare forcings from different mechanisms, on the assumption that similar global-mean forcings produce similar global-mean surface temperature changes. This study illustrates two circumstances where simple models show that the conventional definition of radiative forcing needs refining. These problems arise mainly with the calculation of forcing due to stratospheric ozone depletion. The first part uses simple arguments to produce an alternative definition of radiative forcing, using a time-dependent stratospheric adjustment method, which can give different forcings from those calculated using the standard definition. A seasonally varying ozone depletion can produce a quite different seasonal evolution of forcing than fixed dynamical heating arguments would suggest. This is especially true of an idealised and extreme "Antarctic ozone hole" type scenario where a sudden loss of ozone is followed by a sudden recovery. However, for observed ozone changes the annually averaged forcing is usually within 5% of the forcing calculated using the fixed dynamical heating approximation. Another problem with the accepted view of radiative forcing arises from the definition of the tropopause considered in the second part of this study. For a correct radiative forcing estimate the "tropopause" needs to separate the atmosphere into regions with a purely radiative response and those with a radiative-convective response. From radiative-convective model results it is found that radiative equilibrium conditions persist for several kilometres below the tropopause (the tropopause being defined as where the lapse rate reaches 2 K km^{-1}). This region needs to be included in stratospheric adjustment calculations for an accurate calculation of forcing, as it is only the region between the surface and the top of the convection that can be considered as a single, forced, system. Including temperature changes in this region has a very large effect on stratospheric ozone forcing estimates, and can reduce the magnitude of the forcing by more than a factor of two. Although these experiments are performed using simple climate models, the results are of equal importance for the analysis of forcing-response relationships using general circulation models.

Correspondence to: P.M. de F. Foster

1 Introduction

Many climate change mechanisms can be thought of in terms of a perturbation to the radiative balance of the atmosphere (IPCC 1990, 1992, 1994, 1995). These IPCC reports define a radiative forcing as the change in net radiation at the top of the troposphere. In time the climate system is expected to respond to this forcing to restore the radiative balance. A positive radiative forcing (net increase in irradiance into the surface-troposphere system) tends to warm the surface and a negative radiative forcing tends to cool the surface. What makes radiative forcing such a useful concept is that there is an approximately linear relationship between the global-mean radiative forcing and the global-mean surface temperature change and, provided the radiative forcing is defined correctly, this relationship is relatively unaffected by the forcing mechanism (IPCC 1990, 1994).

This relationship can be written: $\Delta T_S = \lambda \Delta F$ where ΔT_S is the global-mean surface temperature change, ΔF is the global-mean radiative forcing and λ is the climate sensitivity parameter. IPCC (1994) places values of this sensitivity parameter between 0.33 K W^{-1} m^2 and 1.1 K W^{-1} m^2, depending largely on the magnitude of the cloud feedback. This formula allows direct comparison of the potential climate impact from different forcing mechanisms, although there is a question whether global mean forcings from atmospheric changes with strong horizontal and/or vertical variability such as sulphate aerosol and stratospheric ozone can be treated in this manner (IPCC 1994). As stated already one of the caveats for this formula to hold is that the radiative forcing needs to be "appropriately defined" (IPCC 1994). IPCC (1994) then goes on to state: "The radiative forcing of the surface-troposphere

system is the change in net irradiance at the tropopause AFTER allowing for stratospheric temperatures to re-adjust to radiative equilibrium, but with the surface and tropospheric temperatures held fixed at their unperturbed values". This study examines aspects of this definition of radiative forcing.

The stratospheric adjustment process assumes that the time scale of the perturbation causing the radiative forcing is long compared to the time scale for stratospheric adjustment. For the case of stratospheric ozone depletion, where the adjustment process is vital in determining the sign of the forcing (see e.g. IPCC 1992), the ozone change shows a marked seasonal variation, most notably in the Antarctic spring. Section 2 examines how the radiative forcing is modified if this dependence is accounted for, using both an idealised ozone change and ones based on recent trend analyses. Section 3 examines another aspect of the definition of the radiative forcing which has, so far, received little attention. The definition is dependent on how the tropopause is specified. Although a number of definitions of the tropopause exist, they are somewhat arbitrary and are not of obvious relevance to the problem of determining the perturbation of the surface-troposphere radiation budget. This section uses a radiative-convective model to compare forcings calculated using different definitions of tropopause height and then compares the climate sensitivity parameters calculated from these forcings. The narrow band radiative transfer models used in this paper are described in Forster and Shine (1997).

The relationship between radiative forcing and climate change is important particularly as the number and type of proposed radiative forcing mechanisms continues to increase (see especially IPCC 1994). This study addresses two aspects of the calculation of radiative forcing which are amenable to study using relatively simple models. A fuller understanding of the relationship between radiative forcing and climate response requires careful experimentation using general circulation models (GCMs). Recent examples of such work include Cox et al. (1995), Chen and Ramaswamy (1996) and Hansen et al. (1997). The study of Hansen et al. (1997) is of particular relevance as their use of a simplified GCM allows a wide-ranging analysis of the forcing-response relationship. The conclusion from all these studies is that, on a global-mean basis at least, radiative forcing is a useful, although not perfect, concept for estimating the relative importance of different climate change mechanisms and for allowing a first order estimate of the global mean surface temperature response. The results of Hansen et al. (1997) indicate the conditions in which the radiative forcing concept is less appropriate, in their model at least, and draws attention to the possibility of a significant dependence of the cloud feedbacks on the nature of the radiative forcing mechanism.

Nevertheless, the two issues addressed in this work are as relevant to GCM analyses of the forcing-response relationship as they are to the calculation of the forcing in its own right. The results will indicate that if the forcing in the GCMs is not calculated with sufficient care, conclusions about the forcing-response relationship drawn from their results may not be robust.

2 Seasonally dependent forcing

A region of the atmosphere can be thought of as being heated (and cooled) by both transport into and out of the region by the dynamics and the radiative heating (and cooling) in the region. This enables the rate of change of temperature in the region to be written as the sum of dynamical and radiative heating rates:

$$\frac{dT^{o}}{dt} = Q^{o}_{dyn} + Q^{o}_{rad} \tag{1}$$

where the superscript 'o' refers to the unperturbed atmosphere. In the equilibrium state

$$Q^{o}_{dyn} + Q^{o}_{rad} = 0 \tag{2}$$

When the radiative balance of the atmosphere is perturbed, by, for example, a change in greenhouse gas concentrations, Q_{rad} will be altered. In the fixed dynamical heating approximation (FDH), as developed by Ramanathan and Dickinson (1979) and Fels et al. (1980), changes in stratospheric temperatures are calculated with this formula, making two assumptions. The first is that the dynamical heating Q_{dyn} is unchanged following a perturbation to the radiative heating Q_{rad}. The second assumption is that the stratosphere has time to reach an equilibrium state. These assumptions lead to the stratospheric temperatures being computed such that

$$Q'_{rad} + Q^{o}_{dyn} = 0 \tag{3}$$

where Q'_{rad} is the radiative heating in the perturbed atmosphere and $Q^{o}_{dyn} = -Q^{o}_{rad}$.

The assumption of fixed dynamical heating is obviously only an approximation to the actual stratospheric response to the perturbation. Nevertheless, the issue of time dependence raised here is of more general relevance and one likely to carry over to models in which the dynamical response is calculated explicitly.

Lower stratospheric temperatures may take several months to reach this equilibrium state (Fels et al. 1980), during which time both the climate and the perturbation causing the forcing may have substantially evolved. In this section we calculate stratospheric temperatures in a similar fashion to the fixed dynamical heating approximation but we do not assume that the stratosphere is in equilibrium, but rather it is in a seasonally evolving state. The left hand side in Eq. (1) is estimated from climatological data. The radiative heating rate is also calculated using the climatological data and then the dynamical heating rate is calculated as a residual. It is this dynamical heating which is kept constant when the atmosphere is perturbed, allowing the temperature change in the stratosphere to be estimated using the following formula:

$$\frac{dT'}{dt} = Q^{o}_{dyn}(t) + Q'_{rad}(t) \tag{4}$$

where

$$Q^{o}_{dyn}(t) = \frac{dT^{\circ}}{dt} - Q^{o}_{rad}(t).$$

Using Eq. (4) the stratospheric temperatures are stepped forward in time, calculating $Q'_{rad}(t)$ at every time step (1 day). Eventually (usually after about 2 y) the stratospheric temperatures reach a state that is seasonally evolving but the same from year to year. The radiative forcing for each day is then given as the change in net irradiance at the tropopause between these perturbed stratosphere conditions and the unperturbed run. In this study this forcing is called the seasonally evolving fixed dynamical heating (SEFDH) forcing.

With the sudden loss and then recovery of Antarctic stratospheric ozone concentrations in the spring time polar vortex, the lower stratospheric temperatures will not have time to reach equilibrium before the ozone hole has recovered (see Shine 1986). This makes the Antarctic scenario perhaps the most interesting to look at using the SEFDH formalism. For exploratory purposes these forcing calculations were done for clear skies; tropospheric temperatures, ozone and water vapour concentrations as well as the tropopause height, were held fixed throughout the year, at their mid-January values. These simplifications altered the absolute forcing values, by some 30–40%, but had little effect on the relative difference between the FDH and the SEFDH forcing. Radiative forcing and stratospheric temperatures were calculated for each day of the year. The unperturbed stratospheric temperatures were estimated by taking a monthly climatology as representative of the mid-monthly conditions and performing a linear interpolation between these mid-monthly values to obtain stratospheric ozone, temperature and water vapour for each day. A new climatology (Freckleton and Forster 1996), based largely on ECMWF temperature and humidity analyses and SBUV ozone amounts, was used as the basis for these calculations. For these calculations there are 10 levels in the model stratosphere, between 20 and 50 km, with a vertical spacing that varies from about 2 km at the tropopause to 4 km in the upper stratosphere.

In the first test case an idealised "ozone hole" is modelled. During the month of October at 80 °S stratospheric ozone is depleted by 50% between 12–28 km, although in reality the "ozone hole" takes some time to form and then recover. This step change provides an extreme example of lower-stratospheric temperature changes. Figure 1a shows how stratospheric temperatures would be altered using the FDH approximation when the equilibrium temperatures are calculated every day i.e. it is assumed that the new equilibrium temperature can be

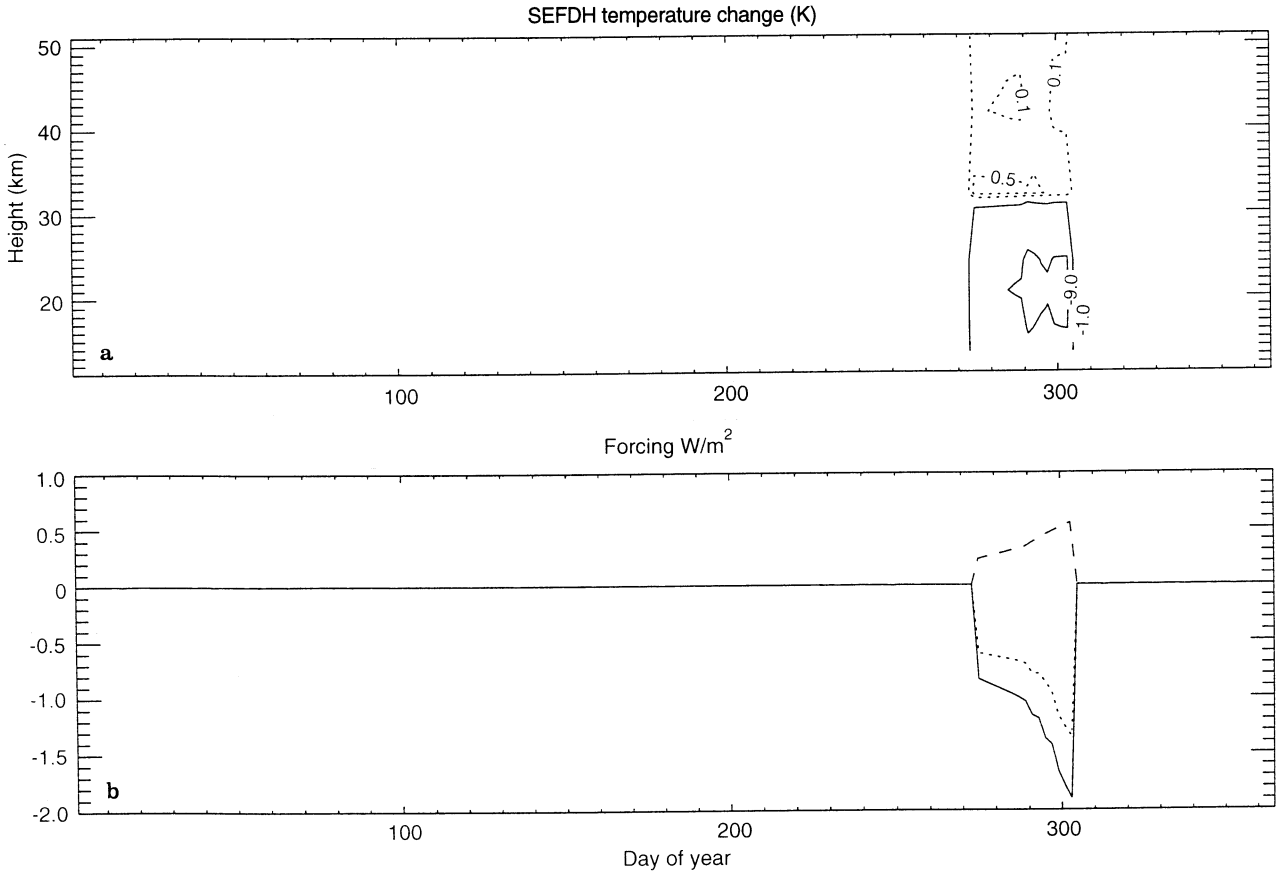

Fig. 1. **a** Stratospheric temperature change (K) from the FDH model as a function of day of the year and height, for 80 °S. Ozone has been depleted between 12–28 km by 50%, during October only. The tropopause is fixed at 12 km and the tropospheric temperatures are fixed at their mid-January values. The contour values are at irregular intervals and are printed on each contour. **b** The shortwave (SW- *dashed line*), longwave (LW-*solid line*) and the net (*dotted line*) radiative forcing (Wm^{-2}) as a function of day of the year at 80 °S from the FDH model, caused by the ozone and temperature changes described in **a**

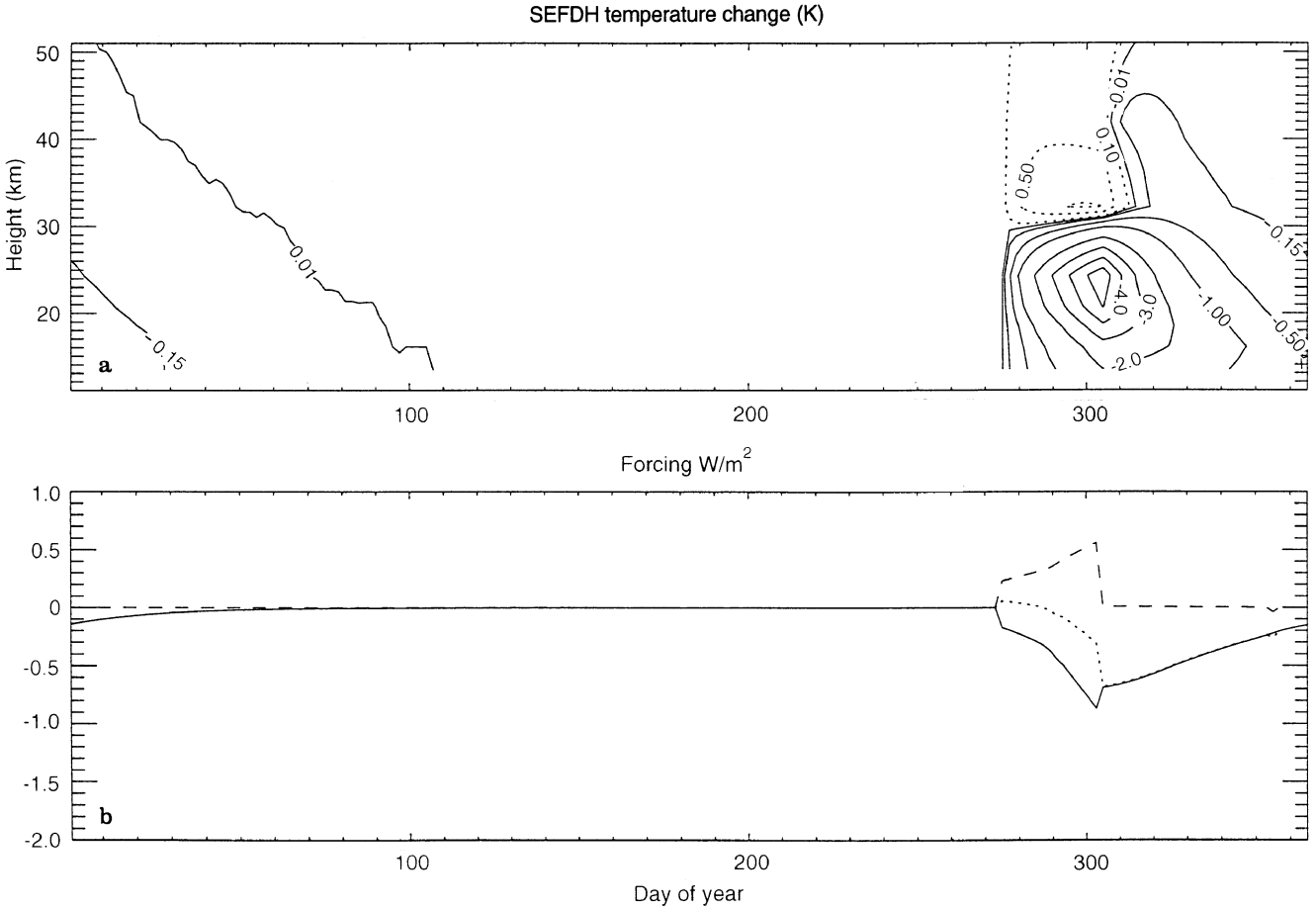

Fig. 2. a Stratospheric temperature change (K) from the SEFDH model as a function of day of the year and height, for 80 °S. Ozone has been depleted between 12–28 km by 50%, during October only. The tropopause is fixed at 12 km and the tropospheric temperatures are fixed at their mid-January values. The contour values are at irregular intervals and are printed on each contour. **b** The shortwave (SW-*dashed line*), longwave (LW-*solid line*) and the net (*dotted line*) radiative forcing (Wm^{-2}) as a function of day of the year at 80 °S from the SEFDH model, caused by the ozone and temperature changes described in **a**

reached, essentially instantaneously. Temperatures are only affected during the period of the ozone depletion; there is a large lower-stratospheric cooling (note the irregular contour interval), of over 8 K, and slight warming above the ozone depletion. The FDH shortwave (SW), longwave (LW) and net forcing is shown in Fig. 1b. Because of the large temperature drop in the lower stratosphere the LW forcing is large and negative and dominates over the SW forcing, making the net forcing negative for the whole month. The net forcing becomes more negative with time. This is the result of two competing effects. The increased availability of sunlight causes an enhanced positive solar forcing. However, because the climatological ozone concentrations are increasing in October, and the simulated ozone hole is a 50% depletion, the absolute ozone depletion is larger at the end of October than at the beginning. This leads to an increase in the perturbation of heating rates in the lower stratosphere which magnifies the local cooling and makes the longwave forcing more negative.

The SEFDH temperature changes and forcings are shown in Fig. 2a and b respectively; a one day time step is used. During October temperature changes above 30 km are very similar to those in Fig. 1a; this is because of the short radiative relaxation time (around 10 days, see e.g. Kiehl and Solomon 1986) at these altitudes. However, in the lower stratosphere the relaxation time is much longer (in excess of a month), with the lower-stratosphere cooling by 4 K towards the end of the month. When the ozone change is turned off at the end of October the cooling extends throughout the stratosphere as temperatures slowly return to their climatological values, which they do so by mid-April.

The forcing pattern in Fig. 2b looks quite different to that in Fig. 1b. The SW forcing is very similar as it is only slightly affected by stratospheric temperatures. The LW forcing, during October, is about 50% of the FDH forcing; this makes the net forcing positive at the start of the month and then it switches sign towards the end of the month. After October the negative LW forcing persists, as the stratosphere remains cooler, and as there is no SW forcing to offset this, the net forcing actually becomes more negative than when the ozone depletion existed; indeed, the forcing remains more negative than its 31 October value until the beginning of December. This leads to the very interesting result that for the annual average,

Table 1. Ratio of SEFDH/FDH net radiative forcing for stratospheric ozone depletions. The ozone depletions are taken from the SBUV total column ozone trend in WMO (1994), except for the idealised case in the final row

	Season				
Latitude (degrees)	DJF	MAM	JJA	SON	Annual average
80 N	0.92	0.96	1.05	1.10	1.02
60 N	0.90	0.93	1.07	1.14	1.00
30 N	0.98	0.99	1.03	1.01	1.00
30 S	1.00	0.98	0.96	1.03	1.00
60 S	1.23	1.03	0.80	0.89	1.01
80 S	1.40	1.24	0.83	0.66	1.03
Idealised 80 S ozone hole	Infinity	Infinity	Infinity	0.76	1.32

the FDH forcing underestimates the SEFDH forcing by 32% (see Table 1). This result went against our original expectations which were that since the FDH approximation produces a larger perturbation to the stratospheric temperatures in October, its annually averaged forcing would be more negative than the SEFDH forcing. It is, however, the months of negative forcing, without the ozone change, which dominate the overall ozone forcing.

To investigate how a more realistic seasonally varying ozone trend would impact on the SEFDH forcing, the SBUV total column ozone trends between 1979–1991 (WMO 1994) were used to calculate radiative forcing at different latitudes. This depletion is assumed to occur in the 7 km directly above the tropopause, with the percentage depletion being held constant with height, in this region. For further details of this methodology see Forster and Shine (1997). An ozone trend for each day was found by linear interpolation of the seasonal ozone trends. Figure 3 shows the SEFDH changes and radiative forcing at 80° S and Fig. 4 shows the SEFDH minus the FDH temperature changes and radiative forcings. The WMO (1994) ozone trends are given in percent decade^{-1} so the temperature changes should be interpreted as trends in K decade^{-1}.

At 80° S during the winter and spring (days 140–330) the SEFDH approximation gives smaller negative temperature trends in the lower-stratosphere by up to 3 K

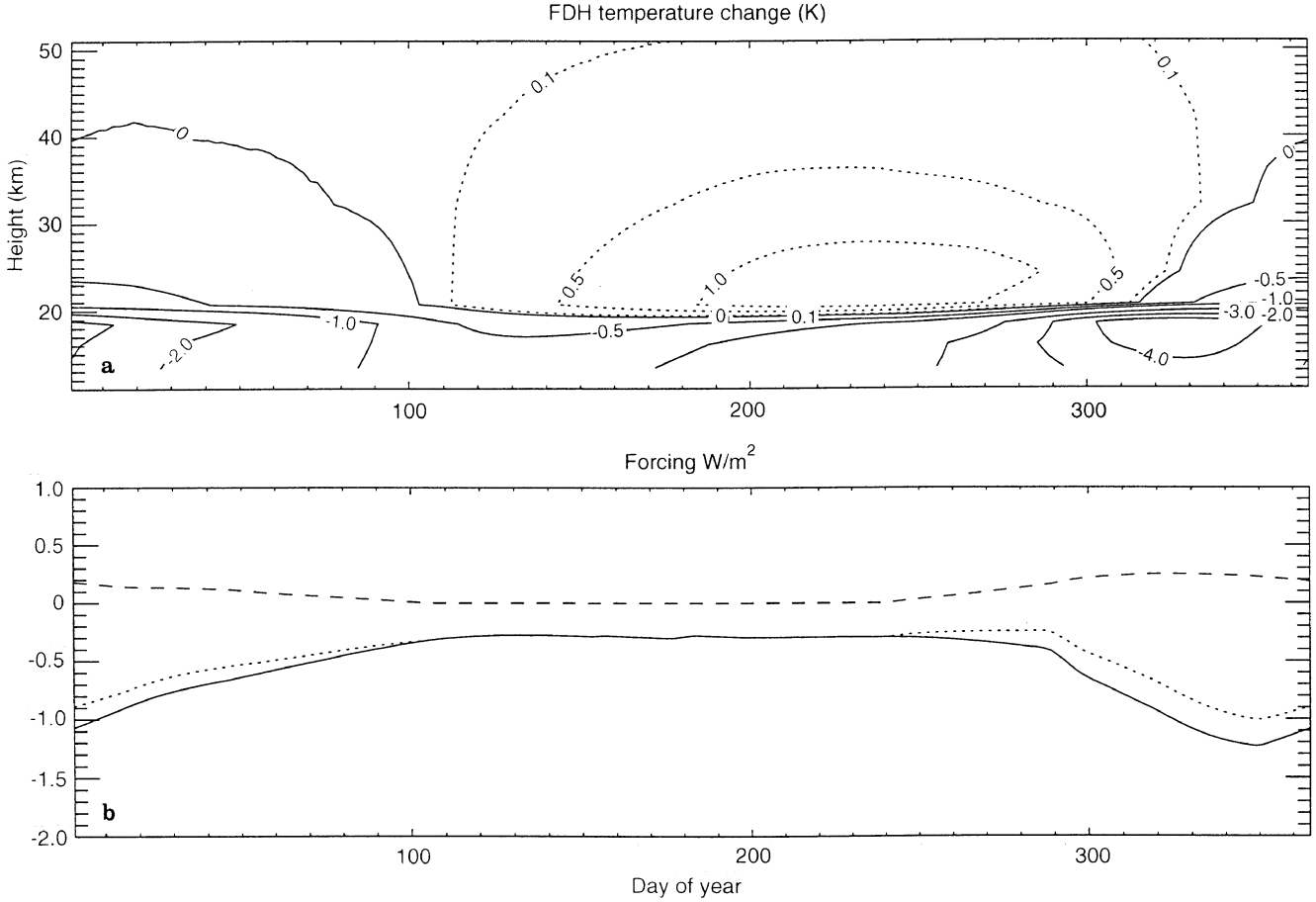

Fig. 3. a Stratospheric temperature change (K) from the SEFDH model as a function of day of the year and height, for 80° S. Ozone has been depleted by the SBUV total column ozone trend between 1979–91 given in WMO (1994). The tropopause is fixed at 12 km and the tropospheric temperatures are fixed at their mid-January values. The contour values are at irregular intervals and are printed on each contour. Since the ozone changes are in%/decade, the temperature change should be interpreted as K/decade. **b** The shortwave (SW-*dashed line*), longwave (LW-*solid line*) and the net (*dotted line*) radiative forcing (Wm^{-2}) as a function of day of the year at 80° S from the SEFDH model, caused by the ozone and temperature changes described in **a**

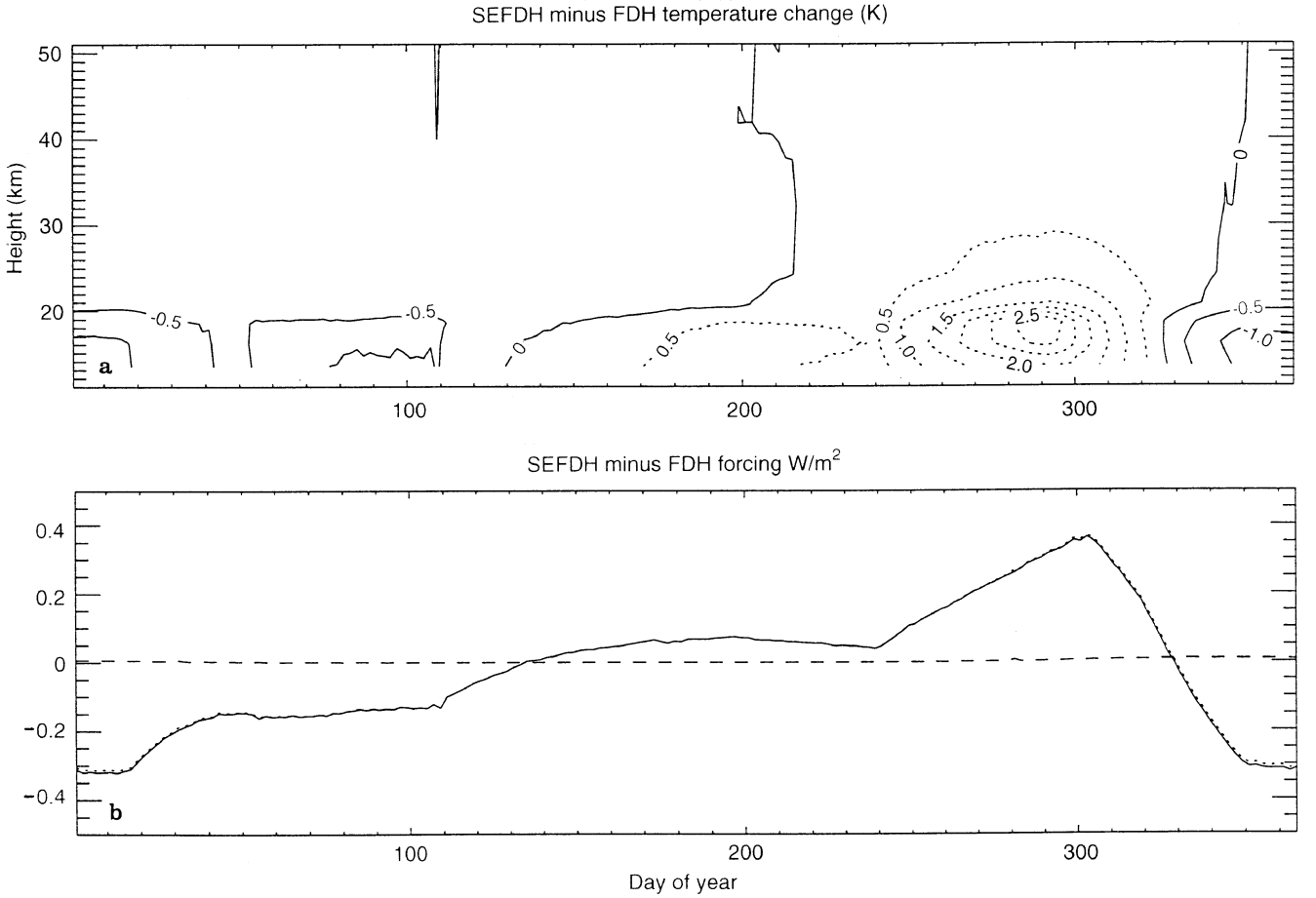

Fig. 4. a The SEFDH minus the FDH stratospheric temperature change (K) as a function of day of the year and height, for 80 °S. Ozone has been depleted by the SBUV trend between 1979–91 given in WMO (1994). The tropopause is fixed at 12 km and the tropospheric temperatures are fixed at their mid-January values. The contour values are irregular intervals. Since the ozone changes are in%/decade, the temperature changes should be interpreted as K/decade. **b** The SEFDH-FDH difference in shortwave (SW-*dashed line*), longwave (LW-*solid line*) and the net (*dotted line*) radiative forcing (Wm-2) as a function of day of the year at 80 °S, caused by the ozone and temperature changes in **a**

decade^{-1} (Fig. 4a). This leads to a more positive forcing over this time period with the SEFDH approximation giving about 60% of the FDH forcing for mid-October (compare Fig. 3b and Fig. 4b). However, in summer and autumn (days 330–140), the SEFDH approximation gives a more negative lower-stratospheric temperature trend (which can exceed 1 K decade^{-1}) (Fig. 4a) which leads to a substantial increase in the negative forcing of 20–40% (compare Figs. 3b and 4b). Differences in forcing are almost entirely due to differences in the longwave forcing as it has a much larger temperature dependence than the shortwave forcing. In the annual average the SEFDH forcing is more negative, but only by 3% (see Table 1). At other latitudes differences in excess of 20% were seen between seasonal forcings, but only very slight differences in the annually averaged forcings were seen (see Table 1).

The results in Table 1 show that although the FDH approximation works very well for the calculation of the annually averaged forcing (differences of 3% or less at all latitudes) the length of the radiative relaxation time means that one season's forcing cannot be considered to be independent of all others. Lower-stratospheric temperatures in one season are influenced by ozone changes in the previous 4–5 months. This has little effect in the tropics and mid-latitudes where the ozone trends are quite constant with season (at 30 °N the SEFDH forcing is less than 5% different than the FDH forcing, for all seasons). However, at high northern and southern latitudes the SEFDH forcing is less negative in winter and spring and more negative in summer and autumn. For example in the northern autumn the SEFDH model gives 10% more negative forcing than the FDH approximation at both 60 °N and 80 °N.

Figure 5a shows the 80 °S FDH and SEFDH temperature changes at 18.5 km (i.e. sections of Figs. 3a and 4a). It can clearly be seen that the SEFDH temperature changes lag behind the FDH temperature by about a month, at this altitude, and have a maximum cooling of smaller magnitude. The SEFDH cooling is, however, more negative than the FDH cooling for almost six months of the year, because it retains the memory of the springtime depletion. A similar plot at 50 km altitude is shown in Fig. 5b. It can be seen that there is now a much smaller

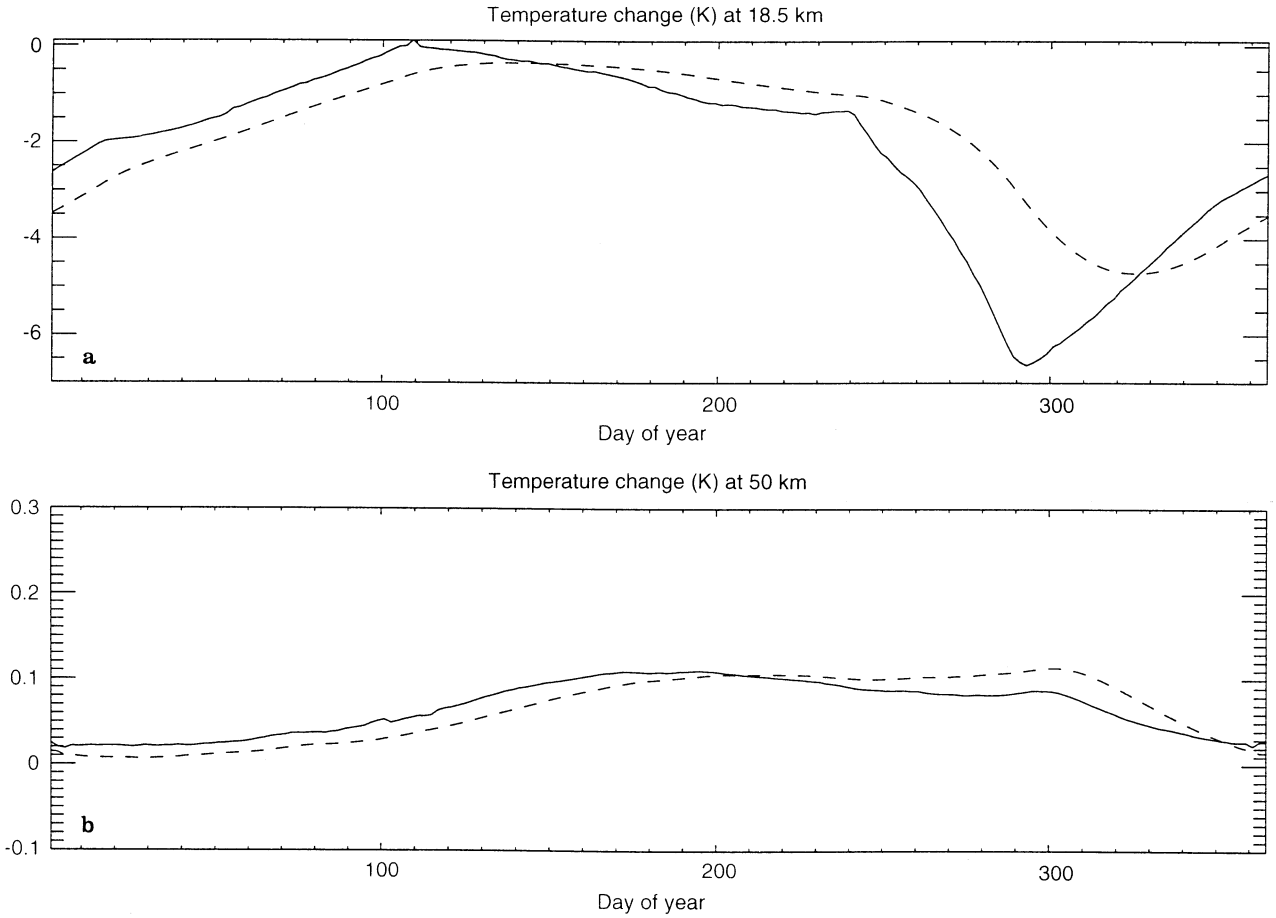

Fig. 5. a The change in stratospheric temperature (K) at 18.5 km as a function of the day of the year at 80 °S. The *dashed curve* is the SEFDH temperature change and the *solid curve* is the FDH temperature change. **b** The change in stratospheric temperature (K) at 50 km as a function of the day of the year at 80 °S. The *dashed curve* is the SEFDH temperature change and the *solid curve* is the FDH temperature change

time lag, of less than a week, between the FDH and SEFDH approach, due to the shorter radiative relaxation times. The difference between the FDH and SEFDH is of clear relevance to studies which compare computed and observed temperature changes. Ramaswamy et al. (1992) and McCormack and Hood (1994) have previously used the FDH approach and noted that the observations lag the FDH temperature changes by roughly a month.

It must be emphasised again that the seasonal evolution of temperature assumes no change in the dynamical heating. In the lower stratosphere (i.e. at levels of most relevance to the radiative forcing) Kiehl et al. (1988) and Mahlman et al. (1994) concluded from GCM studies that the thermal response to an imposed ozone hole is largely radiative in nature. Nevertheless these authors and Cariolle et al. (1990), show that there may be a significant dynamical response. Mahlman et al. (1994) show that the Antarctic ozone loss is accompanied by a hemispheric scale change in the residual circulation in early summer with increased descent and dynamical heating of high latitudes and increased ascent and dynamical cooling at mid-latitudes. The impact of the stratospheric dynamical response on the stratospheric temperatures and hence, on the radiative forcing can not be ascertained using our simple model nor has it yet been calculated using GCM derived temperature changes, to the authors' knowledge.

3 Dependence of forcing on tropopause height

This section examines definitions of the tropopause based on the 1-dimensional thermal structure of the atmosphere. The tropopause can also be defined in dynamical terms, but for the purposes of radiative forcing calculations it is the thermal structure of the atmosphere which is important, so dynamical tropopauses are not discussed here.

Figure 6 shows the equilibrium temperature profile produced by our radiative-convective model (described in the next section). The temperature profile from our own global and annual mean climatology (GAM) (Freckleton and Forster 1996) is plotted alongside this for comparison, as well as the net radiative heating rates in the radiative-convective model. Global mean ozone and cloud data are used in the radiative-convective model, and water vapour concentrations are found using the parametrisation described in the Appendix; carbon dioxide concentrations are set at their pre-industrial value of 279 ppmv (taken from IPCC 1990). The surface albedo has been altered

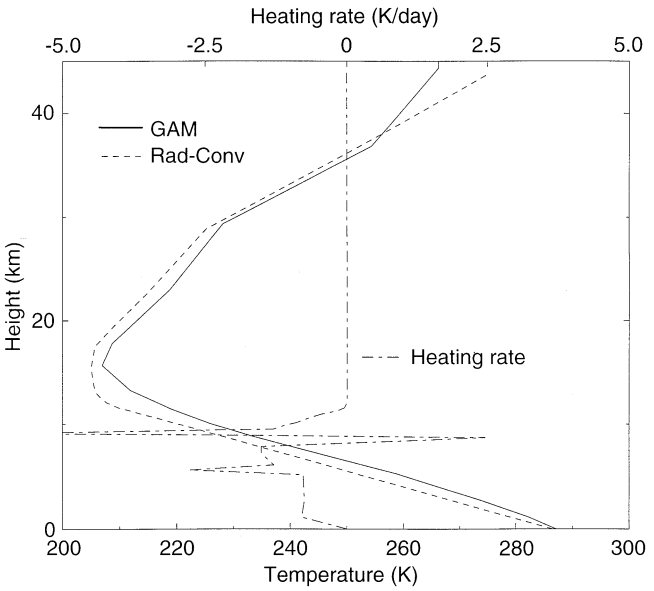

Fig. 6. The temperature (K) of the atmosphere as a function of height, for our global and annual mean atmosphere (*GAM*) and the unperturbed radiative-convective model (*Rad-Conv*) (bottom X-axis). Plotted on the same graph are the net radiative heating rates (K day^{-1}) of the unperturbed radiative-convective model (top X-axis)

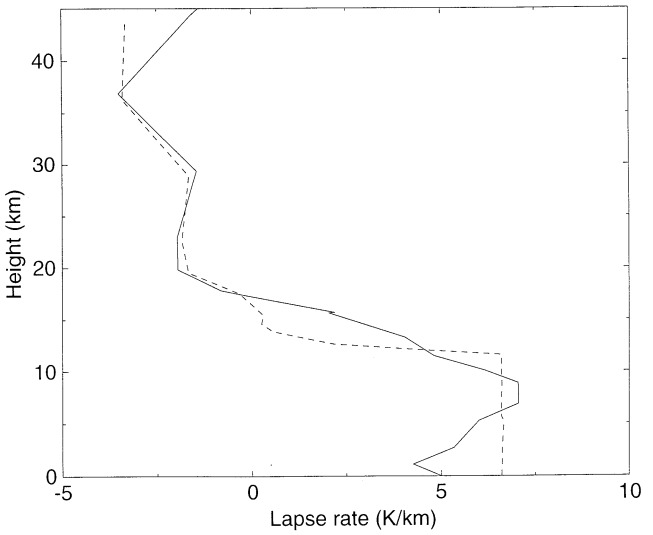

Fig. 7. The lapse rate (K km^{-1}) as a function of height for both the *GAM* atmosphere and the unperturbed radiative-convective model (*Rad-Conv*)

from the climatological value of 0.14 to 0.10 to make the surface temperature in the radiative-convective model close to that of the climatology. Three possibilities for the definition of the tropopause in the radiative-convective model include: (1) the height of the temperature minimum; (2) the height at which the lapse rate is equal to 2 K km^{-1} (following the definition of the tropopause in e.g. WMO, 1985); (3) the height at which the net radiative heating rate reaches zero. The 2 K km^{-1} tropopause was found by linear interpolation between model levels. For the GAM atmosphere the temperature minimum and lapse rate definition give roughly the same tropopause height (at about 16 km). In the radiative-convective model temperature profile the temperature minimum occurs at nearly the same height (16 km) as it does in the GAM profile; the 2 K km^{-1} tropopause occurs at 13 km, some 3 km below its level in the GAM atmosphere. This difference between the heights of the 2 K km^{-1} tropopause could arise from the resolution employed in the two atmospheres: the resolution has been increased to 10 mb in the radiative-convective model, in the region of the tropopause, so it is able to more precisely determine the height of the various tropopauses. The net radiative heating rate tropopause occurs at around 12 km, some 4 km below the temperature minimum definition of the tropopause. Ramanathan and Coakley (1978), Held (1982) and Sinha and Shine (1994) found similar tropopauses in their radiative-convective model studies. For example, Ramanathan and Coakley (1978) found that the top of their convective layer was around 11 km, and their temperature minimum, or a large change in the lapse rate, was some 4 km higher than this. Figure 7 shows lapse rate plotted as a function of height. In the radiative-convective model the top of the convection is easily identified by the sudden change in lapse rate. There is no such sudden change in the GAM atmosphere; the lapse rate steadily increases from about 10 km upwards. This makes it difficult to define the "top of the convective layer" solely based on the GAM temperature profile.

Thuburn and Craig (1997) examined the zonal-mean tropopause height in a GCM and found, in the tropics and subtropics, that the 2 K km^{-1} tropopause was at about 16.5 km (100 mb), while the temperature minimum occurs at around 18 km (80 mb). In addition, the peak of the winter branch of the Hadley circulation occurs at around 13.5 km (160 mb). A "secondary" tropical tropopause, or a considerable stabilisation in the atmosphere at around 13–14 km, has also been noticed by other authors (e.g. Palmén and Newton 1969; Shapiro et al. 1987). Graves (1951) and Defant and Van de Boogard (1963) noticed this "double tropopause" and found that the passage of convective systems altered the height of the lower tropopause without affecting the lapse rate tropopause. These studies provide evidence that the top of the convection in the tropics and subtropics occurs at an altitude lower than the lapse rate definition of the tropopause and that this phenomenon is not just an artefact of radiative-convective models.

Radiative-convective models provide one of the simplest ways of studying climate change. It has been shown (see e.g. IPCC 1994) that, in the absence of feedbacks, the surface temperature change in such a model can be related to the adjusted radiative forcing with a climate sensitivity parameter of around 0.3 K W^{-1} m^2. The instantaneous forcing does not have such a relationship to surface temperature change. For example IPCC (1994) reported the adjusted and instantaneous climate sensitivity parameters for a wide range of forcing mechanisms. The instantaneous sensitivity parameter varied between -1.47 K W^{-1} m^2, for a 50% reduction in ozone between 12 and 40 km, and 0.32 K W^{-1} m^2, for a 1 ppbv increase in CFC-12, whilst the adjusted sensitivity parameter only

varied between 0.30 K W^{-1} m^2 and 0.31 K W^{-1} m^2. From this result it can be seen that if the radiative forcing of various mechanisms are to be compared with each other it is imperative to calculate the adjusted forcing correctly. In a radiative forcing calculation, when performing stratospheric adjustment, it is important to separate regions of the atmosphere with a purely radiative response to those regions with both a dynamical and radiative response. The "forcing" and "response" can then be taken independently of each other with the "forcing" establishing itself over a few months and the climate system taking decades to respond to this forcing. In the radiative-convective model the cut-off between radiative equilibrium and radiative-dynamical equilibrium occurs at the top of the convective layer, well below the common definitions of the tropopause. Defining a radiative forcing at a level higher than the top of the convective layer may lead to an incorrect separation of "the climate forcing" from "the climate response" and therefore lead to an inaccurate calculation of the forcing. This hypothesis is tested in the next section.

The purpose of these experiments is to show how differences in tropopause height affect the radiative forcing. Using a GCM to predict the height of the top of the convection, may lead to different tropopause heights than those calculated from our radiative-convective model. The tropopause would also have a latitudinal and time dependence that our model is unable to represent. Although the forcings might well be different in a GCM, the dependence of the forcing-response relationship to the choice of tropopause level is likely to persist. Hence, the issue of choosing an appropriate tropopause level is equally important for GCM analyses of the forcing-response relationship, so the results here have a wider application than just for the radiative-convective model.

4 Radiative-convective model results

A 1-dimensional radiative-convective model is used to look at the climate response, without any feedbacks, to a variety of different forcings calculated for two different tropopause definitions. The radiative-convective model used is based on that of Sinha and Shine (1994) with the radiation schemes updated to those in Forster and Shine (1997). Water vapour concentrations were given by the water-vapour parametrisation in the Appendix. Although most of the results in this section do not include water-vapour feedback, the parametrisation was used throughout to provide consistency between the water vapour feedback and non-feedback experiments. The model calculates atmospheric heating rates and steps these forward in time. If the lapse rate between two model layers rises above 6.5 K km^{-1} the layer temperatures are adjusted, whilst conserving energy, so the lapse rate equals 6.5 K km^{-1}, following the convective adjustment method of Manabe and Strickler (1964). This process is designed to simulate the role of globally averaged convection.

The experiments are performed in the following way. First the surface temperature response is calculated using the radiative-convective model, following the perturbation of atmospheric constituents. Second the radiative forcing is calculated for comparison with the calculated surface temperature change. Two tropopause heights are considered for the forcing calculations; the temperatures are adjusted only above these heights to return the stratosphere to radiative equilibrium. In this region of radiative equilibrium, the forcing, following the temperature adjustment, is independent of height; i.e. the top of atmosphere forcing is the same as the forcing at the tropopause. The tropopause is either taken as the top of the convection (11.6 km) or at the height of the 2 K km^{-1} lapse rate in the GAM atmosphere (15.8 km). The top of the convection is the natural tropopause in the radiative-convective model, whilst the lapse rate GAM atmosphere tropopause is where, in the absence of the radiative-convective results, one might expect the boundary between the "troposphere" and "stratosphere" to occur, and is the height often used in radiative forcing calculations.

Four climate change experiments were performed to investigate the influence of the choice of tropopause height on the radiative forcing. The experiments were: (1) doubling pre-industrial carbon dioxide concentrations (from 279 to 578 ppmv); (2) adding 1 ppbv of CFC-12; (3) depleting ozone by 50% above the GAM 2 K km^{-1} tropopause; and (4) increasing water vapour concentrations above the top of the convection by 33%. These experiments were not meant to be realistic climate change scenarios but were designed to cover a wide variety of perturbations to the temperature profile, especially in the upper troposphere and stratosphere.

Figure 8 shows the temperature changes produced in the radiative-convective model for the four experiments. Each frame shows three different temperature changes: the solid line corresponds to the forcing calculation where temperatures are adjusted only above the 2 K km^{-1} GAM tropopause (F-2 K); the dotted line is the radiative forcing run allowing temperatures to change above the top of the convective layer (F-CONV); the dashed line is the full radiative-convective model run which calculates temperature changes throughout the atmosphere (FULL).

Figure 8a shows the plot for the carbon dioxide experiment. As expected the FULL run shows a heating of the surface and cooling above 12 km; the forcing runs show the stratospheric cooling, with the F-CONV run producing an extra cooling between the top of the convection and the GAM tropopause, although the F-2 K and F-CONV coolings converge at about 20 km.

For the carbon dioxide experiment (Fig. 8a) the FULL run has smaller coolings, or even warmings, above the top of the convection compared to the F-CONV run. The difference between the F-CONV and the FULL temperature changes above the top of the convection indicate that part of the FULL temperature change, in this region, could be considered as part of the response rather than part of the forcing. The warming of the surface and troposphere leads to an increase in the upwelling thermal infrared irradiance; this increases the energy absorbed in the lower stratosphere, which leads to a warming. This indicates that the transition between warming and cooling, in the cases of increases in CO_2, may depend on the degree to which the troposphere has re-equilibrated with the forcing. Hence this transition height may well be higher in

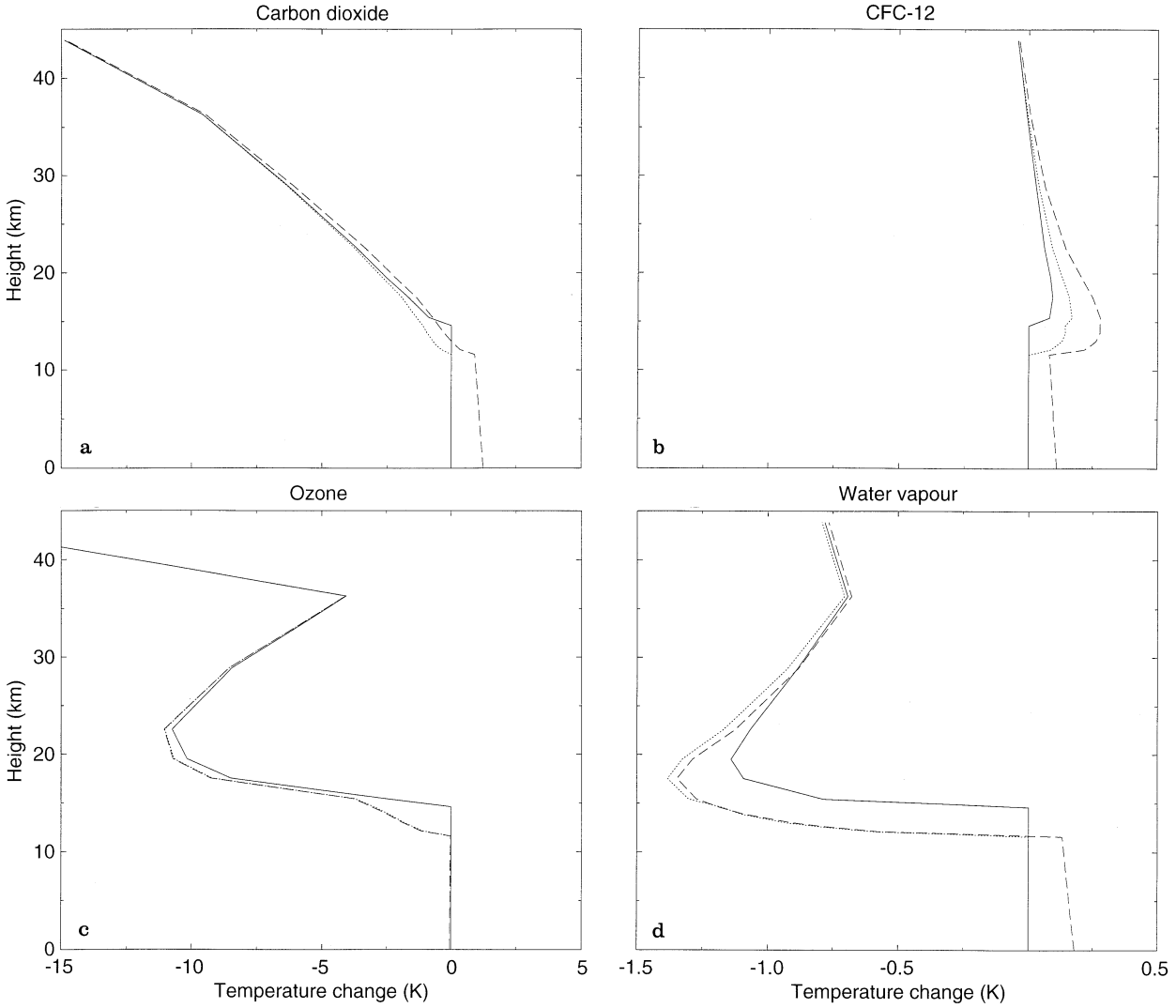

Fig. 8a–d. The temperature change (K) as a function of height calculated by the radiative-convective model. Three runs of the model are shown: *solid line* (F-2 K) with temperature changes only above the 2 K km^{-1} tropopause; *dotted line* (F-CONV) with temperature changes only above the top of the convective layer; *dashed line* (FULL) temperature changes throughout the atmosphere. Four experiments are shown: **a** doubling of pre-industrial carbon dioxide from 279–578 ppmv; **b** adding 1 ppbv of CFC-12; **c** depleting ozone by 50% above the 2 K km^{-1} GAM tropopause; **d** increasing water vapour concentrations by 33% above the top of the convection

equilibrium GCM runs than in either observations or transient GCM studies. It also indicates that the radiative forcing calculated in a model using stratospheric temperatures resulting from a full equilibration of the climate system would not be the same as the forcing calculated prior to equilibration, as part of the effect of the surface-troposphere response would be included in the forcing. The case of CFC-12 (Fig. 8b) shows a similar offset in temperatures between the FULL and F-CONV runs above the top of the convection, whereas the FULL runs for ozone (Fig. 8c) and water vapour (Fig. 8d) have similar temperature changes, above the top of the convection, to the F-CONV runs.

Table 2 shows the forcing for the two tropopause definitions both for the instantaneous case (when the stratospheric temperatures are fixed) and the adjusted case. It also gives the no-feedback climate sensitivity parameter of each case which is the surface temperature change divided by the appropriate forcing.

For carbon dioxide (Fig. 8a) the extra cooling above the top of the convection in the F-CONV case compared to the F-2 K case might, at first sight, be expected to lead to smaller forcing for F-CONV, as the decrease in downwelling irradiance at the respective tropopauses (which acts to reduce the forcing) will be greatest for F-CONV. In fact the opposite is the case (see Table 2) with the F-CONV forcing being 2% greater than the F-2 K forcing. The radiative forcing can be split into two components: the instantaneous change in the net tropopause irradiance and the change in the downwelling tropopause irradiance due to the effect of the adjusted temperatures. The instantaneous change in irradiance at the tropopause is caused by both changes in upwelling and downwelling irradiance. Figure 9 shows how the downwelling minus upwelling

Table 2. Results of four climate change experiments performed with the radiative-convective model, without any feedbacks, described in the text. The table shows the surface temperature change (ΔT_o), and four radiative forcings and their associated climate sensitivity parameters. F-I2 K is the instantaneous forcing calculated at the 2 K km^{-1} tropopause; F-ICO is the instantaneous forcing at the top of the convective layer; F-2 K is the forcing, with adjustment above the 2 K km^{-1} GAM tropopause; F-CONV is the forcing, with adjustment above the top of the convective layer

Experiment	ΔT_o (K)	F-I2K (Wm^{-2}) 2 K km^{-1} (λ) (KW^{-1} m^2)	F-ICO (Wm^{-2}) top of convective layer (λ) (KW^{-1} m^2)	F-2K(Wm^{-2}) 2 K km^{-1} (λ) (KW^{-1} m^2)	F-CONV(Wm^{-2}) top of convective layer (λ) (KW^{-1} m^2)
CO_2: 279–558 ppmv	1.24	4.29 (0.29)	4.47 (0.28)	3.73 (0.33)	3.80 (0.33)
CFC-12: 0–1 ppbv	0.11	0.34 (0.32)	0.29 (0.38)	0.35 (0.31)	0.35 (0.32)
Ozone: 50% depletion in stratosphere	− 0.034	0.95 (− 0.036)	0.93 (− 0.037)	− 0.32 (0.11)	− 0.11 (0.32)
33% increase in water vapour above convection	0.17	0.610 (0.29)	0.90 (0.19)	0.46 (0.39)	0.55 (0.33)

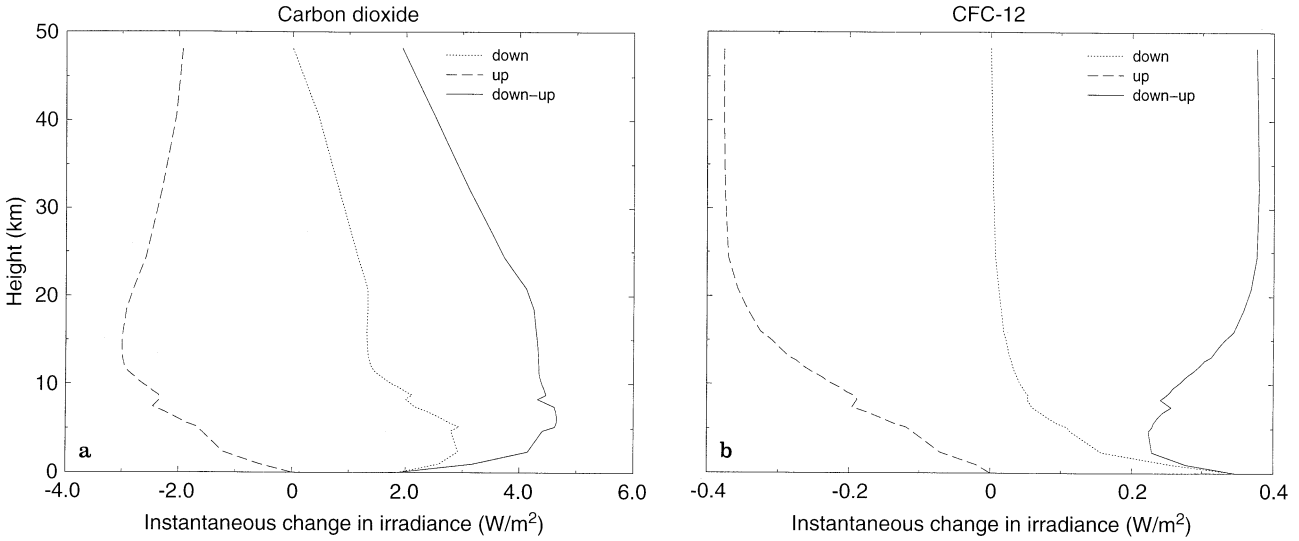

Fig. 9. a The downwelling (*dotted line*), upwelling (*dashed line*) and the downwelling-upwelling (*solid line*) instantaneous change in irradiance (Wm^{-2}) as a function of height for the carbon dioxide experiment. **b** The downwelling (*dotted line*), upwelling (*dashed line*) and the downwelling-upwelling (*solid line*) instantaneous change in irradiance (Wm^{-2}) as a function of height for the CFC-12 experiment

instantaneous changes in irradiance (i.e. forcing) varies as a function of height for the perturbations to CO_2 (Fig. 9a) and CFC-12 (Fig. 9b). Between the two tropopauses (12–16 km), for carbon dioxide, the instantaneous change in upwelling irradiance increases with height at a slightly greater rate than the downwelling change in irradiance decreases. This means the instantaneous forcings decreases with height (see the solid line in Fig. 9), making the instantaneous forcing at the 2 K km^{-1} lapse rate tropopause smaller than the instantaneous forcing at the top of the convection (see columns 3 and 4 of Table 2). Therefore even though the F-CONV radiative forcing is larger than the F-2 K radiative forcing, the F-CONV adjusted radiative forcing has decreased by a larger amount (0.67 Wm^{-2}) than the F-2 K adjusted forcing (0.56 Wm^{-2}), when compared to their respective instantaneous forcings; this is consistent with the extra cooling in the F-CONV run, seen in Fig. 8.

In the absence of temperature changes above the 2 K km^{-1} tropopause, the difference between the two instantaneous forcings will determine whether the region between the two tropopauses will cool or warm in the F-CONV run. If the 2 K km^{-1} tropopause has a more positive instantaneous forcing than the instantaneous forcing at the top of the convection, as in the CFC-12 case (see the solid line in Fig. 9b and Table 2), there is a net flux of energy into this region and it will warm up (see Fig. 8b). Carbon dioxide (Fig. 8a) and water vapour (Fig. 8d) have a larger instantaneous forcing at the top of the convection than at the 2 K km^{-1} tropopause (Table 2); this implies a net flux of energy out of the region and leads to a cooling in the region between the two tropopauses.

Ozone depletion (Fig. 8c), by the same arguments, would be expected to warm this region in the F-CONV run; but the strong cooling above the 2 K km^{-1}

tropopause means that there is considerably less downwelling emission into the region between the two tropopauses and this leads to a strong cooling that is not apparent when looking at the instantaneous forcings. The effect of this strong cooling above the 2 K km^{-1} tropopause can be seen in Table 2 from the fact that the 2 K km^{-1} forcing decreases from $+0.95$ Wm^{-2} to -0.32 Wm^{-2} following adjustment; this is sufficient to cause the layer between the tropopauses to cool.

As well as showing radiative forcings, Table 2 also shows surface temperature changes and climate sensitivity parameters. In this simple radiative convective model the two instantaneous forcings are associated with a wide range of climate sensitivity parameters; the 2 K km^{-1} instantaneous sensitivity parameter varies between -0.04 K W^{-1} m^2 for the ozone depletion experiment to 0.32 K $W^{-1}m^2$ CFC-12 experiment. This agrees well with the range in IPCC (1994) and again emphasises that the instantaneous forcing is not adequate as a way of comparing the effects from different mechanisms of climate change. The F-2 K climate sensitivity parameters still show a large variation, between 0.11 K W^{-1} m^2 and 0.39 K W^{-1} m^2, with the ozone and water vapour changes producing the extreme sensitivity parameters. Using the F-2 K radiative forcing and a sensitivity parameter of 0.3 K W^{-1} m^2 as an indicator of surface temperature change would lead to an over-estimation of the effect of stratospheric ozone depletion (by a factor of three) and a 25% under-estimate of the effect of increases in upper tropospheric and stratospheric water-vapour. However, the F-CONV sensitivities are all very similar and only vary between 0.32 KW^{-1} m^2 and 0.33 K W^{-1} m^2 making this the only forcing that produces similar sensitivities for all four climate change experiments. Using a sensitivity parameter of 0.32 KW^{-1} m^2 to predict surface temperature changes from the F-CONV forcing would give less than a 2% error. However, it needs to be kept in mind that these are the surface temperature changes from a radiative-convective model without feedbacks; a GCM and the real world may well have different climate sensitivities for different forcing mechanisms of the same magnitude (see Hansen et al. 1997).

To test whether these results depend on the presence of feedbacks, the experiments were repeated using water vapour feedback (using the method in the appendix) and/or a different critical lapse rate (based on a moist adiabat, after Sinha and Shine 1994). Using water vapour feedback did not affect the forcings but magnified all the temperature changes, and sensitivity parameters, by about 90%. Using a moist adiabat for the critical lapse rate increased the forcing, for the water vapour perturbation experiment by about 20%. Using a moist adiabat in the other experiments had little (less than 5%) effect on the forcings and stratospheric temperature changes. The surface temperature changes, and hence the sensitivity parameters, for the moist lapse rate experiments were roughly 55% of those in the 6.5 K km^{-1} lapse rate experiments presented in Table 2 (in line with the study of Sinha and Shine 1994). Earlier work in Forster and Shine (1997) found that a simple mixed layer ocean and latent heat release had little effect on the radiative-convective model response. These extra experiments emphasised the robust nature of these results in the context of a radiative-convective model.

5. Summary

Many of the results in this work have focused on the radiative forcing calculation for a lower stratospheric ozone depletion; this is perhaps the most interesting case to study as the stratospheric temperature adjustment plays a crucial role in determining the magnitude and even the sign of the forcing. However it needs to be stated that wherever a large change in lower stratospheric temperatures is expected, for example when looking at the effects of volcanic aerosols, similar problems with the radiative forcing calculation would be expected to occur.

A new way of performing stratospheric adjustment has been developed that does not require the stratosphere to be in instantaneous equilibrium. Calculating the radiative forcing, using this technique, the seasonally evolving fixed dynamical heating approximation (SEFDH), produces forcings (in the annual average) of a slightly higher magnitude than the normally used fixed dynamical heating (FDH) approximation. For a sudden loss of ozone in October at 80 °S the SEFDH model produces a 32% more negative annually averaged forcing. For a smoothly varying, with season, ozone depletion (taken from SBUV 1979–1991), differences between the annually averaged SEFDH and FDH forcings are small (less than 4%). However, differences of up to 40% can still be seen in the seasonal radiative forcing at high latitudes. For any forcing mechanism that produces large changes in lower-stratospheric temperatures and acts over short time scales (such as volcanic eruptions) the SEFDH approximation may well give a very different forcing than the FDH approximation, and give a better indication of how the climate would be expected to respond, both in terms of forcing the surface-troposphere system and altering the lower stratospheric temperature response.

Using a 1-D radiative-convective model, radiative forcings and surface temperature changes were calculated for four climate change experiments, in the absence of climate feedbacks. Two different definitions of tropopause height were used in the calculation of radiative forcing: (1) the tropopause is where the lapse rate is 2 K km^{-1}; (2) the tropopause is at the top of the convection, as simulated by the radiative-convective model.

In the radiative-convective model the top of the convective layer was about 4 km below the 2 K km^{-1} tropopause. To calculate the radiative forcing, the radiative-convective model adjusts the stratospheric temperatures until the atmosphere above the tropopause is in radiative equilibrium. The height difference between the two tropopauses leads to radiative forcings and climate sensitivities which depend on tropopause definition. Stratospheric ozone changes and upper tropospheric and stratospheric water vapour changes lead to the largest differences in forcing between the tropopauses. For the experiments undertaken, the climate sensitivity parameter was nearly constant (at 0.32 K W^{-1} m^2) when the tropopause was defined as the top of the convective layer. When the tropopause was taken at the height of the 2 K km^{-1} lapse

rate, the climate sensitivity parameter was not constant, but varied between 0.11 K W^{-1} m^2, for stratospheric ozone depletion, and 0.39 K W^{-1} m^2, for upper tropospheric and stratospheric water vapour increases. This shows that in the radiative-convective model, at least, comparing the 2 K km^{-1} tropopause radiative forcing of different climate change mechanisms, is not a good indication of surface temperature change. But the radiative forcing concept works well if the tropopause is taken as the top of the convective layer.

This study has shown that unless care is taken to correctly distinguish the part of the atmosphere in a purely radiative-equilibrium state from the rest of the atmosphere the applicability of the radiative forcing concept breaks down, and the prediction of a surface temperature change from the radiative forcing becomes unreliable. Unless the height of the tropopause is chosen carefully, in both radiation models and GCMs, it will be very difficult to calculate radiative forcing, from ozone changes especially, with any degree of accuracy. This perhaps accounts for some of the reasons for such large uncertainties in the calculation of the radiative forcing associated with ozone changes. It is undoubtedly simpler to identify different tropopauses in a radiative-convective model than it would be at a particular location or time in a GCM. Nevertheless, this work indicates that the 2 K km^{-1} tropopause may not be the most appropriate, and it may be better to choose the lowest level at which the radiative heating becomes the dominant diabatic term.

Appendix

Manabe and Wetherald (1967) developed a parametrisation scheme to approximate atmospheric water vapour mass mixing ratios from values of pressure and temperature. The approximation is described next.

First relative humidities (rh) are approximated by a function of pressure (p):

$$rh = 0.77\ (p \times 10^{-3} - 0.02)/0.98$$

where pressure has units of mb.

Saturation vapour pressures are calculated through an empirical relationship with temperature (T), from Murray (1967). A default mass mixing ratio of 6.0×10^{-6} is assumed for low pressures for which the relative humidity approximated becomes negative and therefore non-physical. Using monthly mean climatological temperature and water vapour data (Freckleton and Forster 1996) it was found that this approximation for calculating water vapour mass mixing ratios could be improved.

We tuned the water vapour parametrisation such that when pressures and temperatures from the climatology were used as input, the calculated water vapour mass mixing ratios were in better agreement with the water vapour data in the climatology. Only the relative humidities needed to be recalculated giving slightly larger values, where:

$$rh = 0.77\ (p \times 10^{-3} - 0.02)/0.75$$

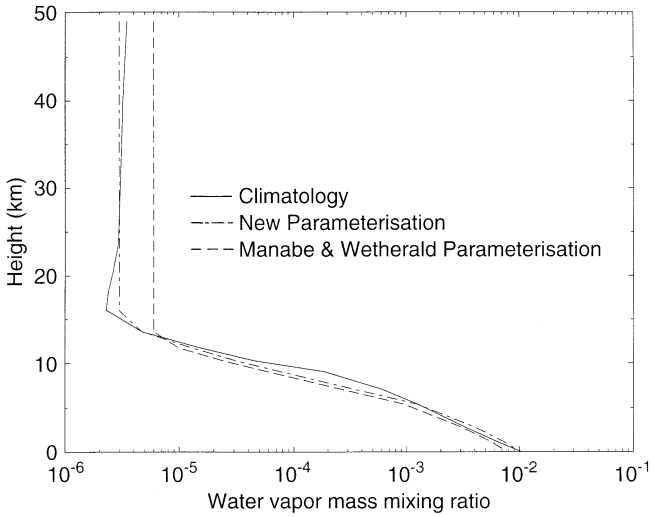

Fig. A1 Water vapour mass mixing ratio as a function of height. The Manabe and Wetherald (1967) parametrisation (*dashed line*), the new parametrisation (*dotted and dashed line*) and the climatological values (*solid line*) are plotted

A notable feature of this expression is that the global-mean relative humidity exceeds 100% at the surface. The difference between this and the standard Manabe and Wetherald (1967) expression occurs because of the averaging process. Manabe and Wetherald's value resulted from a global average of the relative humidity. Our value was produced by taking a global value of the specific humidity and calculating the relative humidity using the global mean temperature profile. For radiative calculations this is more appropriate as it is the mass of water that is most important. However, in practical terms (e.g. the strength of the water vapour feedback) we found little difference in the results using the different averaging procedures.

The default value of mass mixing ratio has also been changed to 3.0×10^{-6} and this default value, applied at pressures less than or equal to 100 mb. Figure A1 shows that the new approximation of the global and annual mean water vapour profile more closely resembles that of the climatology.

Acknowledgements. Piers Forster was funded under EC grant EC54-CT94-0492 and a UK NERC grant GR3/10435. Rebecca Freckleton was funded under a UK NERC grant GR3/9327. Eleanor Highwood is thanked for her helpful discussion. We thank the referees for useful comments.

References

Cariolle D, Lasserre-Bigorry A, Royer JF and Geleyn JF (1990) A general circulation model simulation of the springtime Antarctic ozone decrease and its impact on mid-latitudes. J Geophys Res 95:1883–1898

Chen CT, Ramaswamy V (1996) Sensitivity of simulated climate perturbations in low-cloud microphysical properties.1. Globally uniform perturbations. J Clim 9:1385–1402

Cox SJ, Wang WC, Schwartz SE (1995) Climate response to radiative forcing by sulphate aerosols and greenhouse gases. Geophys Res Lett 22:2509–2512

Defant F, Van de Boogard HME (1963) The global circulation features of the troposphere between the equator and 40 N based on a single day's data. Part I: the structure of the basic meteorological fields. Tellus 15 : 251–260

Fels SB, Mahlman JD, Schwarzkopf MD, Sinclair RW (1980) Stratospheric sensitivity to perturbations in ozone and carbon dioxide: radiative and dynamical response. J Atmos Sci 37 : 2265–2297

Freckleton RS, Forster PM de F (1996) A three dimensional climatology. Radiation Group internal report 1. Available from: Keith Shine, Department of Meteorology, Reading University, Reading, RG6 6BB, UK

Forster PM de F, Shine KP (1997) Radiative forcing and temperature trends from stratospheric ozone depletion. J Geophys Res 102 : 10841–10855

Graves ME (1951) The relation between the tropopause and convective activity in the subtropics (Puerto Rico). Bull Am Meteorol Soc 32 : 54–60.

Hansen J, Sato M, Ruedy R (1997) Radiative forcing and climate response. J Geophys Res 102 : 6831–6864

Held IM (1982) On the height of the tropopause and the static stability of the troposphere. J Atmos Sci 39 : 412–417

IPCC (1990) Climate change (1990) The IPCC scientific assessment. Houghton JT, Jenkins GJ, Ephraums JJ (eds) Cambridge University Press, Cambridge, UK, Chap. 2

IPCC (1992) Climate change (1992) The Supplementary report to the IPCC scientific assessment. Houghton, JT, Callander BA Varney SK (eds). Cambridge University Press, Cambridge, UK, pp 47–69

IPCC (1994) Climate change (1994) Radiative forcing of climate change and an evaluation of IPCC IS92 emission scenarios. Houghton JT, Meira Filho LG, Bruce J, Hoesung Lee, Callander BA, Haites E, Harris N, Maskell K (eds) Cambridge University Press, Cambridge, UK, pp 167–199

IPCC (1995) Climate change (1995) The science of Climate change. Houghton JT, Meira Filho LG, Bruce J, Callander BA, Haites E, Harris N, Kattenberg A, Maskell K (eds), Cambridge University Press, Cambridge, UK, Chap. 2

Kiehl, JT, Solomon S (1986) On the radiative balance of the stratosphere, J Atmos Sci 43 : 1525–1534

Kiehl JT, Boville BA, Briegleb BP (1988) Response of a general circulation model to a prescribed Antarctic ozone hole. Nature 332 : 501–504

Mahlman JD, Pinto JP, Umscheid LJ (1994) Transport, radiative and dynamical effects of the Antarctic ozone hole: a GFDL "SKYHI" model experiment. J Atmos Sci 51 : 489–508

Manabe S, Strickler RF (1964) Thermal equilibrium of the atmosphere with a convective adjustment. J Atmos Sci 21 : 361–385

Manabe S, Wetherald RT (1967) Thermal equilibrium of the atmosphere with a given distribution of relative humidity. J Atmos Sci 24 : 241–259

McCormack JP, Hood LL (1994) Relationship between ozone and temperature trends in the lower stratosphere: latitudinal and seasonal dependences. Geophys Res Lett 21 : 1615–1618

Murray FW (1967) On the computation of saturation vapour pressure. J Appl Meteorol 6 : 203–204

Palmén E, Newton CW (1969) Atmospheric circulation systems. Academic Press, New York

Ramanathan V, Coakley JA, Jr (1978) Climate modelling through radiative-convective models. Rev Geophys Space Phys 16 : 465–489

Ramanathan V, Dickinson RE (1979) The role of stratospheric ozone in the zonal and seasonal radiative energy balance of the Earth-troposphere system. J Atmos Sci 36 : 1084–1104

Ramaswamy V, Schwarzkopf MD, Shine KP (1992) Radiative forcing of climate from halocarbon-induced stratospheric ozone loss. Nature 355 : 810–812

Sinha A, Shine KP (1994) A one dimensional study of possible cirrus cloud feedbacks. J Clim 7 : 158–173

Shapiro M A, Hampel T, Krueger AJ (1987) The Arctic tropopause fold, Month Weather Rev 115 : 444–454

Shine KP (1986) On the modelled thermal response of the Antarctic stratosphere to a depletion of ozone. Geophys Res Lett 13 : 1331–1334

Thuburn J, Craig GC (1997) GCM tests of theories for the height of the tropopause. J Atmos Sci 54 : 869–882

WMO (1994) Scientific assessment of ozone depletion, 1994. World Meteorological Organization, Global Ozone Research and Monitoring Project - Rep 37, Geneva